

## Multi-dimensional respiratory motion tracking from markerless optical surface imaging based on deformable mesh registration

This article has been downloaded from IOPscience. Please scroll down to see the full text article.

2012 Phys. Med. Biol. 57 357

(<http://iopscience.iop.org/0031-9155/57/2/357>)

View [the table of contents for this issue](#), or go to the [journal homepage](#) for more

Download details:

IP Address: 195.220.108.5

The article was downloaded on 20/12/2011 at 06:44

Please note that [terms and conditions apply](#).

# Multi-dimensional respiratory motion tracking from markerless optical surface imaging based on deformable mesh registration

Joël Schaerer<sup>1,2</sup>, Aurora Fassi<sup>3</sup>, Marco Riboldi<sup>3,4</sup>, Pietro Cerveri<sup>3</sup>,  
Guido Baroni<sup>3,4</sup> and David Sarrut<sup>1,2</sup>

<sup>1</sup> CREATIS, CNRS UMR 5220, INSERM U1044, Université Lyon 1, INSA-Lyon, Villeurbanne, France

<sup>2</sup> Department of Radiotherapy, Centre Léon Bérard, Lyon, France

<sup>3</sup> Department of Bioengineering, Politecnico di Milano, Milano, Italy

<sup>4</sup> Bioengineering Unit, CNAO Foundation, Pavia, Italy

E-mail: [aurora.fassi@mail.polimi.it](mailto:aurora.fassi@mail.polimi.it)

Received 20 July 2011, in final form 12 October 2011

Published 14 December 2011

Online at [stacks.iop.org/PMB/57/357](http://stacks.iop.org/PMB/57/357)

## Abstract

Real-time optical surface imaging systems offer a non-invasive way to monitor intra-fraction motion of a patient's thorax surface during radiotherapy treatments. Due to lack of point correspondence in dynamic surface acquisition, such systems cannot currently provide 3D motion tracking at specific surface landmarks, as available in optical technologies based on passive markers. We propose to apply deformable mesh registration to extract surface point trajectories from markerless optical imaging, thus yielding multi-dimensional breathing traces. The investigated approach is based on a non-rigid extension of the iterative closest point algorithm, using a locally affine regularization. The accuracy in tracking breathing motion was quantified in a group of healthy volunteers, by pair-wise registering the thoraco-abdominal surfaces acquired at three different respiratory phases using a clinically available optical system. The motion tracking accuracy proved to be maximal in the abdominal region, where breathing motion mostly occurs, with average errors of 1.09 mm. The results demonstrate the feasibility of recovering multi-dimensional breathing motion from markerless optical surface acquisitions by using the implemented deformable registration algorithm. The approach can potentially improve respiratory motion management in radiation therapy, including motion artefact reduction or tumour motion compensation by means of internal/external correlation models.

(Some figures may appear in colour only in the online journal)

## 1. Introduction

Motion tracking is a key aspect in external beam radiotherapy, especially when applied to extra-cranial sites where breathing motion is relevant (Keall *et al* 2006). Accuracy in motion tracking is crucial in order to ensure accurate dose delivery to a moving target. The required accuracy level strictly depends on the applied motion mitigation strategy, and it is maximal when the target is tracked continuously over its trajectory (Verellen *et al* 2010).

External motion tracking in radiotherapy typically relies on non-invasive infrared devices to capture the motion of the patient surface (Meeks *et al* 2005). External motion is used for patient setup, to monitor breathing motion and to check that a patient does not move excessively during irradiation (Baroni *et al* 2006). It can be utilized as a surrogate for internal motion for accurate 4D CT reconstruction, or with modern radiation therapy delivery technologies for motion compensated treatments (Gianoli *et al* 2011, Hoogeman *et al* 2009, Depuydt *et al* 2011).

Many different methods have been proposed to monitor the external surface motion. Perhaps the most widespread clinical solution is the Real-time Position Management (RPM) system from Varian Medical Systems (Palo Alto, CA), which monitors the motion of a single object placed on the patient's abdomen (Ford *et al* 2002). Such a method does not accurately depict the complexity of patient motion: breathing motion, whole body motion, thoracic or abdominal breathing. In order to give more detailed information, systems requiring the use of several passive markers placed on the patient have been proposed (Meeks *et al* 2005, Baroni *et al* 2006, Wagner *et al* 2007). Even though these systems feature good accuracy and yield motion tracking at specific anatomical landmarks, they typically involve long patient preparation and may not be repeatable due to inaccuracy in marker placement (Wang *et al* 2001). The Cyberknife Synchrony system (Accuray Inc., Sunnyvale, CA) relies for example on the use of three optical markers attached to a wearable vest for the estimation of the external respiratory signal (Kilby *et al* 2010), requiring however additional equipment for the patient, which may also imply relative motion between the skin and the tracking markers.

Optical systems that do not require markers exist, such as the AlignRT/GateCT (VisionRT Ltd, London, UK), the Sentinel system (C-RAD AB, Uppsala, Sweden) and the Galaxy system (LAP Laser, Lüneburg, Germany) (Bert *et al* 2005, Brahme *et al* 2008, Moser *et al* 2011). These devices provide the 3D reconstruction of the external surface of the patient as a function of time. However, the geometrical representation of the surface changes over time, meaning that vertices and edges of the meshes acquired at different time stamps vary. This is due to the fact that surface detection is performed by projecting structured light over a moving surface from a fixed point of view. Therefore, such systems do not provide a direct measure of local motion at specific surface landmarks. External surface motion can be derived by applying a surface registration procedure in order to establish the correspondence between a source and a target mesh. When surface registration is applied to the thoraco-abdominal patient surface, registration procedures need to account for a deformation model to adequately describe the motion due to breathing. This means that the transformation that warps each vertex of the source surface onto its corresponding point on the target is not rigid. The existing optical tracking systems currently implement rigid surface fitting procedures which provide a global surface motion, without taking deformation effects explicitly into account. This approach does not allow us to capture local surface transformations and complex breathing motion patterns, which generally vary for different regions of the thoraco-abdominal surface.

One of the most well-known algorithms for surface registration is called Iterative Closest Point (ICP) and was introduced by Besl and McKay (1992). This algorithm is limited to rigid or affine transformations. Feldmar and Ayache (1996) were among the first to propose

a method that allows for deformable transformations. They initially perform regular ICP to get a rough alignment between the source and target surfaces. They then relax the rigidity constraint by computing affine transformations for spherical subsets of the source surface. Regularization is performed by geometrically smoothing the resulting affine transforms. Allen *et al* (2003) proposed a regularization term based on connectivity rather than spatial proximity. Assuming the source surface is represented as a mesh, each vertex is attributed a different affine transformation, with a global constraint penalizing large differences between transformations of connected points. Amberg *et al* (2007) showed that this problem can be solved directly using a least-squares approach. The resulting algorithm resembles ICP in that it optimizes correspondences and transformations sequentially, with the difference that it searches for one affine transformation per vertex of the source mesh instead of a global transformation.

In this paper we investigated the potentiality of deformable mesh registration to track breathing motion over the thoraco-abdominal surface at specific landmarks, making use of current technologies for real-time surface imaging in radiotherapy. We analysed the method performance as a function of the main structural parameters of the algorithm and quantify the accuracy in multi-dimensional respiratory tracking.

## 2. Methods and materials

### 2.1. Deformable surface registration algorithm

In order to extract the multi-dimensional breathing motion of the thoraco-abdominal surface from markerless optical imaging, we implemented a non-rigid surface registration algorithm. Therefore, we were able to provide a point by point mesh correspondence by taking into account the surface deformation induced by respiration. The implemented approach is based on the non-rigid ICP method developed by Amberg *et al* (2007).

The standard ICP algorithm consists of an iterative optimization of a global transformation: at each step, each vertex  $v_i$  of the source surface  $S$  is matched to the closest vertex on the target surface  $T$ , and the corresponding displacements are used to estimate a global rigid or affine transformation, using a linear least-squares approach. The extension of this process to cope with deformation implies the estimation of one affine transformation  $X_i$  ( $3 \times 4$  matrix) for each vertex in  $S$ . Minimizing the distance between the deformed source  $X_i v_i$  and the target surface leads us to consider the following first term of a general cost function:

$$E_d(X) = \sum_{v_i \in V} w_i \text{dist}^2(T, X_i v_i), \quad (1)$$

where  $V$  is the set of source vertices and  $w_i$  are the weights attached to each vertex. The weight  $w_i$  is set to 1 if a minimal distance correspondence is found and 0 otherwise. In order to ensure the convergence of the algorithm towards the correct solution and to avoid false registration, specific constraints are introduced, choosing reasonable thresholds for the proposed application. Unrealistic surface point correspondences are excluded by verifying the following criteria:

- the estimated displacement should not be too tangent to the surface, with a maximum deviation angle from the surface normal of  $30^\circ$ ;
- the displacement norm should not exceed a fixed limit, equal to 10 cm;
- the angular difference between the source and target surface normals should be lower than  $30^\circ$ .

The issue of assigning an affine transform to each vertex makes the cost function under-constrained and the optimization problem ill-posed. In order to overcome this drawback,

an additional regularization term is considered in the overall cost function, by adding up constraints to the free variables in the  $X_i$  transform set. This constraint represents the transition smoothness across adjacent transforms which can be modelled as

$$E_s(X) = \alpha \sum_{\{i,j\} \in \varepsilon} \|(X_i - X_j)\|_F^2, \quad (2)$$

where  $\varepsilon$  is the set of edges of  $S$  and  $\alpha$  is the stiffness factor that modulates the capabilities of the surface to deform. This term is used to penalize the difference between the transformations of neighbouring vertices under the Frobenius norm  $\|\cdot\|_F$ , thus regularizing the surface deformation and correctly constraining the equation system. The general cost function is derived by summing equations (1) and (2). This can be rearranged to obtain the linear equation system:

$$E(X) = \|AX - B\|_F^2 \quad (3)$$

which is solved directly using a least-squares approach. In order to obtain an efficient solution for the resulting linear system, the matrix  $A$  is factorized using the Cholesky decomposition.

The implemented non-rigid ICP algorithm consists of two iterative loops. In the outer loop, the stiffness factor  $\alpha$  is gradually decreased with uniform steps, starting from higher values, which enables recovery of an initial rigid global alignment, to lower values, allowing for more localized deformations. For a given value of  $\alpha$ , the problem is solved iteratively in the inner loop. At each step, the closest point on the target mesh is computed for each point in the source surface and the optimal set of affine transforms for this correspondence is estimated. The inner iterative process stops when the norm of the difference between two consecutive transforms  $X$  is lower than a threshold  $\delta$ . The convergence threshold is adapted for each outer loop step, setting  $\delta$  equal to a constant fraction of the norm of the transform difference computed in the first inner iteration.

## 2.2. Experimental validation

The accuracy of the proposed deformable registration method in tracking external breathing motion from markerless surface imaging data was assessed in five male healthy volunteers, reproducing the realistic clinical setting of the proposed application. Static surface acquisitions were performed by means of the AlignRT optical system (figure 1(a)), with the subject lying in supine position on a standard treatment couch. For each volunteer, the thoraco-abdominal surface (figure 1(b)) was acquired at three different phases of the breathing cycle: maximum inhale, maximum exhale and an arbitrarily chosen intermediate position. Two subjects repeated the experiments twice, resulting in seven full data sets for method validation. For each acquisition session, the three surfaces corresponding to different respiratory phases were pair-wise registered, acting alternately as source and target mesh. This allows us to increase the number of registrations available as validation data set, leading to 6 registrations per subject experiment, for a total of 42 registrations. The AlignRT software was used only for data acquisition, whereas the implementation and evaluation of the deformable registration algorithm were realized through our own software developed in C++. Eigen libraries were used to solve the linear system for the estimation of surface point transformations, while all other computations regarding surface processing and method evaluation were based on Insight Toolkit (ITK) and Visualization Toolkit (VTK) libraries (Ibáñez *et al* 2005, Schroeder *et al* 2006).

The accuracy of the implemented registration algorithm was quantified in terms of residual surface distance, by evaluating the Euclidean distance between each point of the deformed source mesh and the closest point on the corresponding target surface. We also estimated the registration error based on the known position of multiple surface control landmarks.

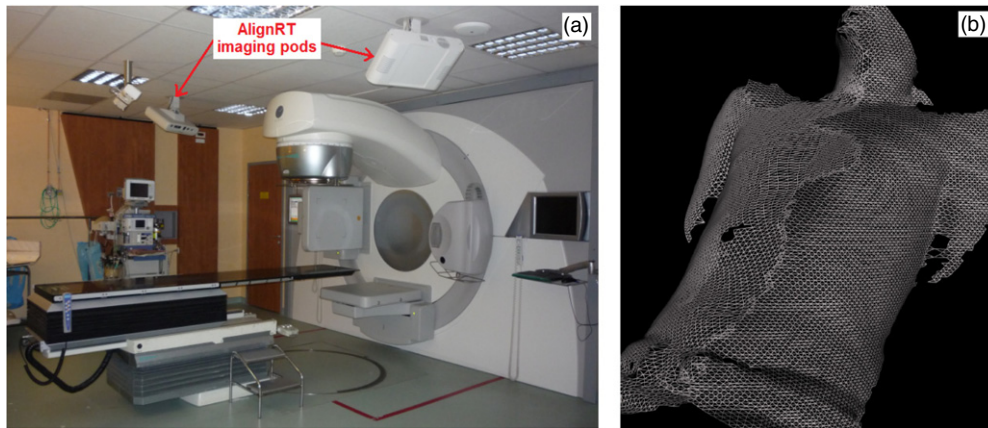


**Figure 1.** (a) AlignRT optical system installed in the radiotherapy treatment room where subject acquisitions were performed. The system is composed of two imaging pods placed symmetrically with respect to the treatment couch. Data from both pods are merged to form an integrated surface model (b).

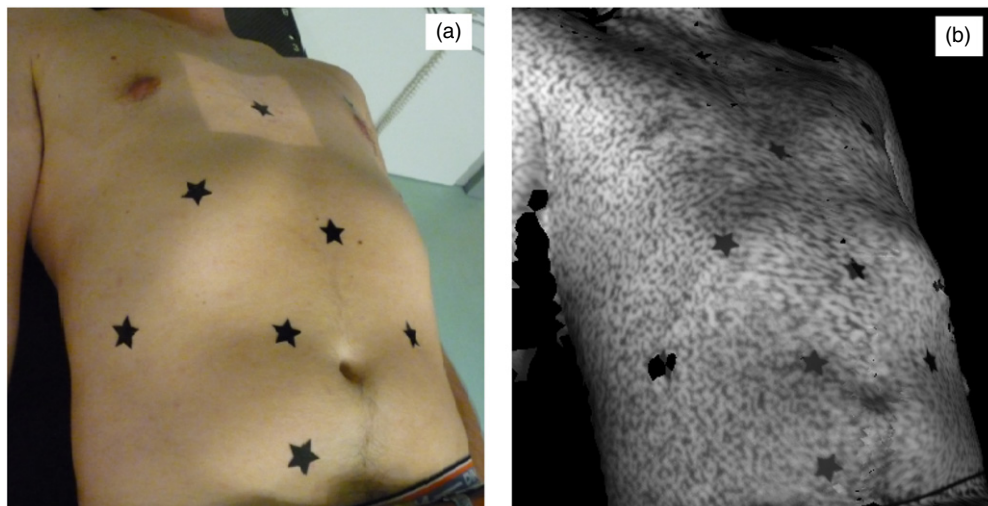


**Figure 2.** (a) Star-shaped black markers placed on the thoraco-abdominal surface of a test subject. (b) Corresponding textured mesh acquired with the AlignRT optical system, showing the structured light pattern projected on the subject surface. Due to the presence of holes in the reconstructed mesh, the marker on the rightmost part of the abdomen could not be identified.

Ten black star-shaped markers were placed on different parts of the thorax and abdomen of the subjects (figure 2(a)). The texturing capabilities of the AlignRT system, providing the grey level representation of the reconstructed meshes, were used for the visualization and identification of the control points (figure 2(b)). Such textured information is available only for static mesh acquisition. The vertices of the star-shaped markers were manually selected on the acquired textured surfaces, and the centroids of each marker were computed by averaging the corresponding vertices. Depending on the marker location for the different subjects, the

number of visible vertices that could be identified in all three breathing phases ranged between 26 and 40, with an average number of 36.4. In order to assess the intra-operator variability in marker identification, the manual clicking of the star vertices on a reference textured surface was repeated ten times by a single operator. The inter-operator variability was instead evaluated by comparing the positions of the star vertices selected by five different operators on the three surfaces acquired for a test subject.

The registration error was computed as the difference between the real displacement of the control points selected on the textured surfaces and the motion estimated through the deformable registration algorithm. In order to account for the discretization of the acquired meshes, the landmarks selected on the source and target surfaces were projected on the respective meshes. The real marker motion was computed from the projected points, whereas the estimated marker motion was obtained by considering the three neighbouring vertices of the source mesh triangle that includes the projected landmark. The displacements of the neighbouring vertices derived from deformable mesh registration were linearly interpolated to estimate the landmark motion.

The performance of the implemented algorithm was separately evaluated for the markers located in the abdominal and thoracic regions, that were manually distinguished using the costal margin as the separation line. The error components for each spatial direction were estimated, and the correlation between the overall registration accuracy and the direction of marker motion was established. The accuracy of deformable mesh registration in localizing surface control markers was compared with the performance of rigid surface registration based on a standard ICP algorithm (Besl and McKay 1992). A sensitivity analysis of the structural parameters of the developed algorithm was also carried out by analysing the registration errors computed over the entire acquisition data set as a function of the following variables: (a) start and final values of the stiffness factor  $\alpha$ ; (b) number of iteration steps in the outer loop; (c) value of the convergence threshold  $\delta$ . The computational cost of the implemented deformable registration algorithm was finally evaluated for all data sets, assessing the correlation with the mean number of vertices in the acquired surfaces.

### 2.3. Method evaluation on patient data

The implemented deformable registration algorithm was applied to real patient data in order to evaluate the method feasibility in recovering multi-dimensional breathing motion from markerless optical surface acquisitions. The VisionRT system in the single pod-based modality (GateCT) was used to continuously acquire the dynamic thoraco-abdominal surface of selected patients during lung cancer radiotherapy treatments (figure 3(a)). The implemented deformable surface registration was applied to obtain the correspondence between an arbitrarily chosen reference surface, represented by the first mesh of the sequence, and the following surfaces. The estimated 3D trajectories of the surface points included in the thoraco-abdominal region of interest (figure 3(b)) were used to derive a multi-dimensional breathing signal. The respiratory surface motion along the three spatial directions was obtained by averaging the individual coordinates of the extracted corresponding surface points. Principal component analysis (PCA) was applied for each direction and the first principal component scores associated with each point were used to evaluate the surface regions that mostly contribute to the breathing signals extracted along the different directions. The estimated motion of the thoracic and abdominal surface regions was also compared to the respiratory signal provided by the GateCT system. This signal is computed as the mean anterior–posterior trajectory of the surface points included in a region of interest selected by the user.

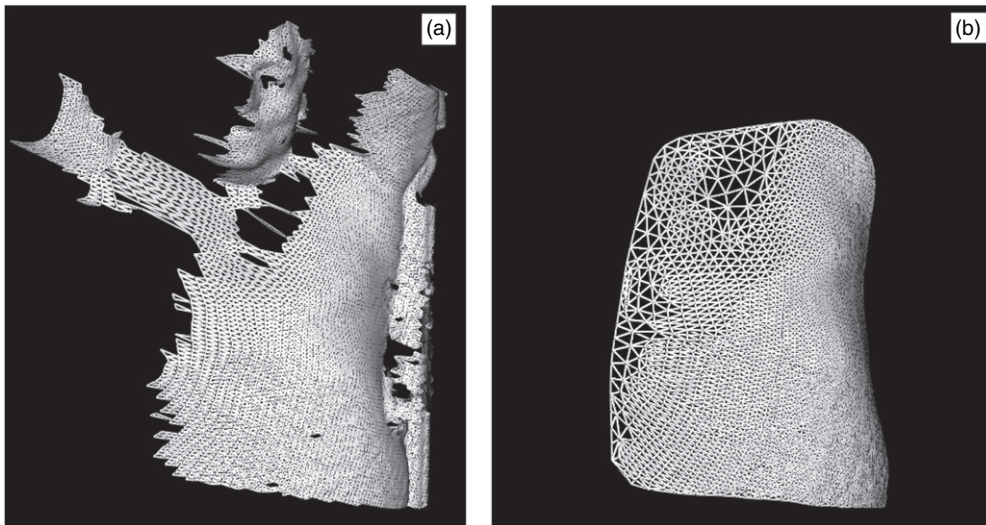


**Figure 3.** (a) Patient surface acquired with the GateCT optical system. The reconstructed mesh is not symmetric, since only a single imaging pod is used for the dynamic surface acquisition in order to achieve a higher frame rate ( $\sim 7$  Hz). (b) Thoraco-abdominal region of interest obtained with the deformable registration algorithm, which is able to smoothly fill the surface holes.

### 3. Results

#### 3.1. Experimental validation

**3.1.1. Intra- and inter-operator variability in marker selection.** Figures 4(a) and (b) show the results related to the intra-operator variability in the repeated identification of the star-shaped markers on a reference textured surface. The intra-operator variability in the selection of the star vertices (figure 4(a)) was computed as the difference between the vertex coordinates manually clicked by the operator and the reference positions defined in the first test. The variability in the identification of the star centroids from the corresponding vertices is also reported (figure 4(b)). The 75th percentile of the error distribution computed for all repeated tests proved to be 0.43 mm for vertex selection and 0.22 mm for centroid identification.

The variability in marker selection performed by five different operators is reported in figures 4(c) and (d). The positions of the star vertices identified by the first operator on the three acquired surfaces of a selected subject were taken as reference to compute the inter-operator variability. The 75th percentile of the resulting errors was 0.80 mm in the case of vertex selection and 0.46 mm in the case of centroid identification. According to the obtained results, the accuracy of the registration algorithm was estimated using the identified position of the star centroids, featuring a lower intra- and inter-operator variability. Since the centroid coordinates defined by the different operators did not prove to be significantly different (Kruskal–Wallis nonparametric test,  $p$ -value = 1), the registration errors were computed by considering the centroid position identified by a single operator as ground truth.

**3.1.2. Sensitivity analysis of algorithm parameters.** Figure 5 depicts the results of the sensitivity analysis performed on the main structural parameters of the implemented algorithm. The registration error, expressed as the median error in the identification of the marker position

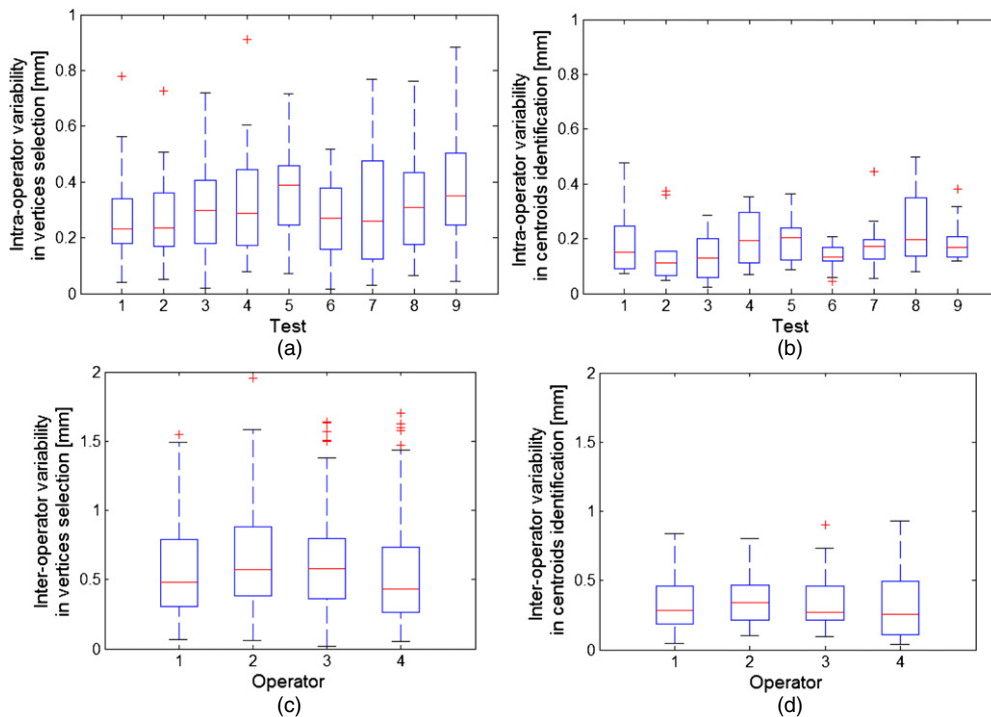


**Figure 4.** Intra- and inter-operator variability in the manual selection of the marker vertices on the textured surfaces (a)–(c) and in the identification of the star centroids from the corresponding vertices (b)–(d). Boxplots depict the 25th, 50th (median) and 75th percentiles of the error distribution for the repeated tests. Whiskers extend from both sides of the box up to 100% of the quartile range and symbols (+) denote outliers.

for all test subjects, was computed by varying one parameter at a time. The analysed variables include the start and final values of the stiffness factor  $\alpha$  (figures 5(a) and (b)), the number of iteration steps in the outer loop (figure 5(c)) and the threshold  $\delta$  for the convergence of the inner iterative processes (figure 5(d)). The registration errors resulting from the sensitivity analysis ranged between 1.61 and 1.69 mm. In the next section, the outcomes of the algorithm corresponding to the best registration accuracy will be analysed in detail. These results were obtained by using 25 outer iteration steps, with a stiffness factor ranging from 150 to 1 and a convergence threshold of 1/100.

**3.1.3. Accuracy and computational performance of deformable surface registration.** Table 1 summarizes the results related to the computational cost of the implemented deformable surface registration algorithm, applied to the acquired data set of healthy subjects. For each acquisition session, the table reports the number of surface vertices averaged over the three acquired breathing phases and the mean time associated with a single iteration of the registration algorithm in the outer loop. The computational performance of the developed application was evaluated using a 2.53 GHz Intel Core 2 Duo processor. The CPU time required per outer iteration ranged between 6.1 and 11.9 s and proved to be linearly correlated with the number of vertices in the registered meshes (Pearson correlation coefficient = 0.9,  $p$ -value < 0.01).

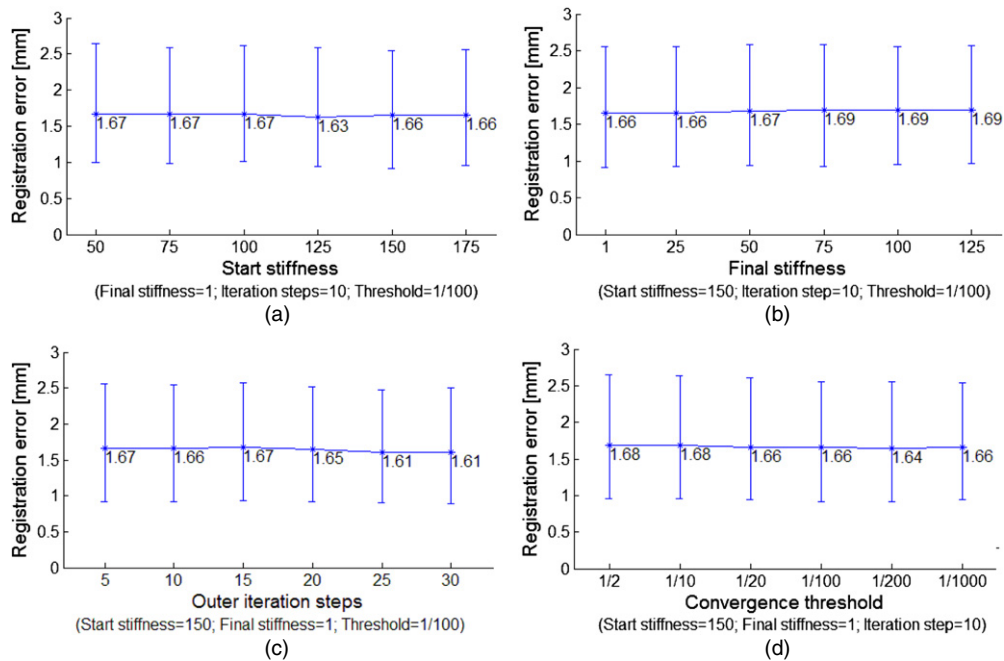


**Figure 5.** Registration errors (median  $\pm$  quartile) in the identification of the marker centroids for the entire data set, as a function of the start stiffness factor (a), final stiffness factor (b), number of iterations in the outer loop (c) and convergence threshold for inner iterations (d).

**Table 1.** Computational performance of the implemented deformable surface registration algorithm. The acquisitions of the two subjects who performed the test session twice are identified by A1, A2 and M1, M2.

Acquisition ID	Mean number of points/surface	Mean computational time/outer loop iteration (s)
A1	9922	9.5
A2	9896	8.8
JA	9820	8.8
JO	10 854	10.1
MA	14 457	11.9
M1	8427	6.1
M2	8410	6.8

The accuracy of the implemented deformable registration algorithm is reported in table 2. For each subject, the table shows the 95th percentile of the residual distance between the deformed source and the target surface after performing mesh registration, as well as the median value of marker localization errors, computed by using as ground truth the position of the control points derived from the textured information. Surface and marker distances in the initial condition and after rigid mesh registration are also listed in table 2. The 95th percentile of the residual surface distance with the developed deformable approach did not exceed 1.20 mm, whereas the median errors on marker localization ranged between 1.05 and 2.27 mm. By applying rigid registration procedures, the median error computed over the entire acquisition data set proved to be 4.21 mm, with residual surface distances ranging from 3.40 to 8.10 mm.

**Table 2.** Residual surface distance (95th percentile) and marker localization errors (median value) for the implemented deformable registration algorithm, compared to the performance of rigid mesh registration and to the initial surface and marker distances.

Acquisition ID	Initial condition		After rigid registration		After deformable registration	
	Surface distance (mm)	Marker distance (mm)	Surface distance (mm)	Marker distance (mm)	Surface distance (mm)	Marker distance (mm)
A1	7.53	5.33	8.10	6.43	0.76	2.07
A2	7.20	3.80	6.07	5.65	0.78	2.27
JA	4.08	2.75	3.40	2.92	0.48	1.39
JO	5.59	3.40	3.67	3.68	0.40	1.05
MA	3.91	2.45	3.41	2.14	1.08	1.36
M1	6.70	3.26	4.35	4.15	1.20	1.52
M2	7.53	4.05	4.65	4.22	1.14	1.84
Total value	6.13	3.59	4.18	4.21	1.08	1.61

Figure 6 shows the surface overlap computed for different breathing phases of a test subject before and after deformable registration. The greater surface distances are localized along the central line that merges the surface models reconstructed by the two imaging pods of the AlignRT optical system. The merging process generates disconnected components near the mesh boundaries, resulting in higher registration errors. Optimized surface stitching algorithms can be used to increase mesh connectivity, thus improving the regularization step of the registration method.

The spatial variability of the registration accuracy on the thoraco-abdominal surface is illustrated in figure 7. The error in marker localization introduced by the registration algorithm is separately plotted for the control points located in the thoracic and abdominal surface regions. The median value of the registration errors computed for all control points over the entire data set was 1.61 mm, whereas it varied from 2.13 mm considering only the thoracic markers to 1.09 mm for the landmarks in the abdominal region. The error distributions estimated for the thoracic and abdominal control points proved to be significantly different (Wilcoxon rank sum test,  $p$ -value  $< 0.01$ ).

The accuracy of the implemented registration algorithm was also evaluated as a function of the anatomical direction. The median error in the localization of all control points measured 1.12, 0.66 and 0.29 mm in the superior–inferior (SI), right–left (RL) and anterior–posterior (AP) directions, respectively. Figure 8 shows the registration errors computed along each anatomical direction as a percentage of the total summed error. The SI component is predominant (59%) for the localization error of the thoracic markers, whereas the landmarks in the abdominal region feature a higher registration error in the RL direction (43%). The percentage error in the AP direction proved to be lower than 20% for all control points. Finally, a significant linear correlation was found between the total registration error and the marker motion in the SI direction (Pearson correlation coefficient = 0.7,  $p$ -value  $< 0.01$ ). The correlation results between the registration accuracy and the motion direction for an exemplificative subject acquisition are depicted in figure 9.

### 3.2. Method evaluation on patient data

Figure 10 shows the multi-dimensional breathing signal extracted from the dynamic thoraco-abdominal surfaces of a lung cancer patient using the implemented deformable surface

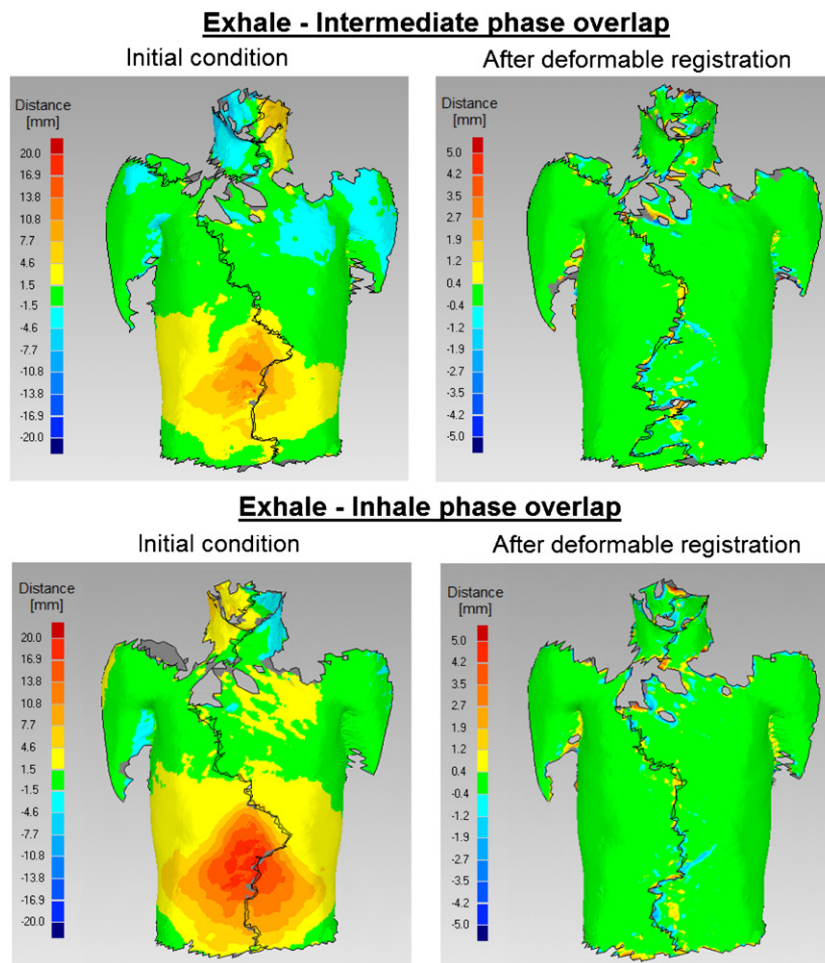


**Figure 6.** Surface overlap at different breathing phases before and after deformable registration. The colour-based intensities represent the surface distance in the initial condition (left panels) and after performing deformable registration (right panels). As can be noticed in this figure, the implemented registration algorithm is also able to recover head rotations.

registration algorithm. The signals depicted in the lower panels of the figure represent the mean surface motion in the three spatial directions, obtained by averaging the SI, RL and AP coordinates of the corresponding surface points generated by the algorithm. Twelve breathing cycles of the patient could be identified, for a total acquisition time of 40 s. The contribution of each surface point to the respiratory signals in the different anatomical directions is represented in the upper panels of the figure. This contribution is computed through PCA analysis, by projecting in the principal component space the surface point motion along different directions.

Figure 11 shows the respiratory signal acquired with the GateCT system during a lung cancer treatment, compared to the AP motion estimated with deformable registration for three surface points selected in the thoracic and abdominal regions. While the GateCT system provides the respiratory information on a limited surface patch, the proposed method yields the 3D motion of any points on the thoraco-abdominal surface. This approach allows us to

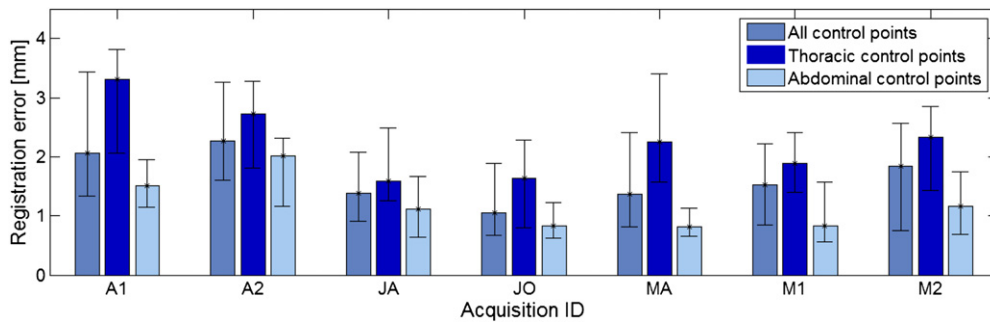


**Figure 7.** Spatial variability of the registration errors (median  $\pm$  quartile), separately estimated for markers located in the thoracic and in the abdominal surface regions.

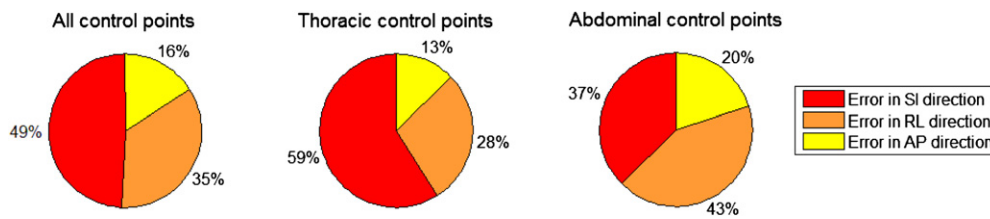


**Figure 8.** Localization errors for thoracic and abdominal control points along different anatomical directions, expressed as a percentage of the summed error.

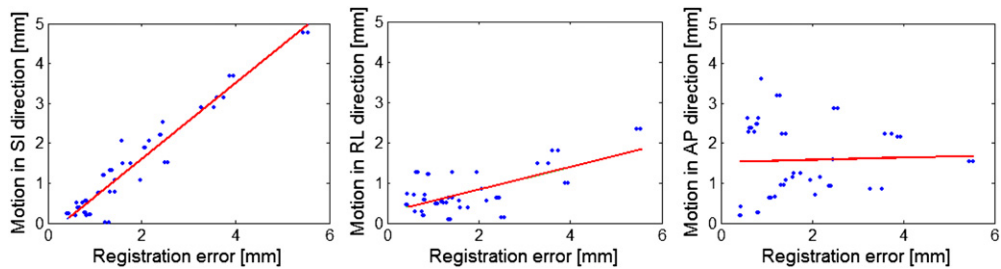


**Figure 9.** Registration errors computed for subject acquisition MA as a function of the marker motion in the three different spatial directions. The linear regression line is overlaid the sample data.

capture the patient specific respiratory patterns of the thorax and abdomen, which generally feature different amplitude and phase shifts.

#### 4. Discussion

The performance of deformable mesh registration in tracking multi-dimensional breathing motion from markerless optical surface acquisition has been specifically investigated. The implemented method was adapted from the optimal step non-rigid ICP algorithm proposed by Amberg *et al* (2007), adding further optimization criteria to increase efficiency and robustness, such as the Cholesky factorization and the exclusion of bad correspondences specifically designed for the proposed application. The accuracy and the computational performance of

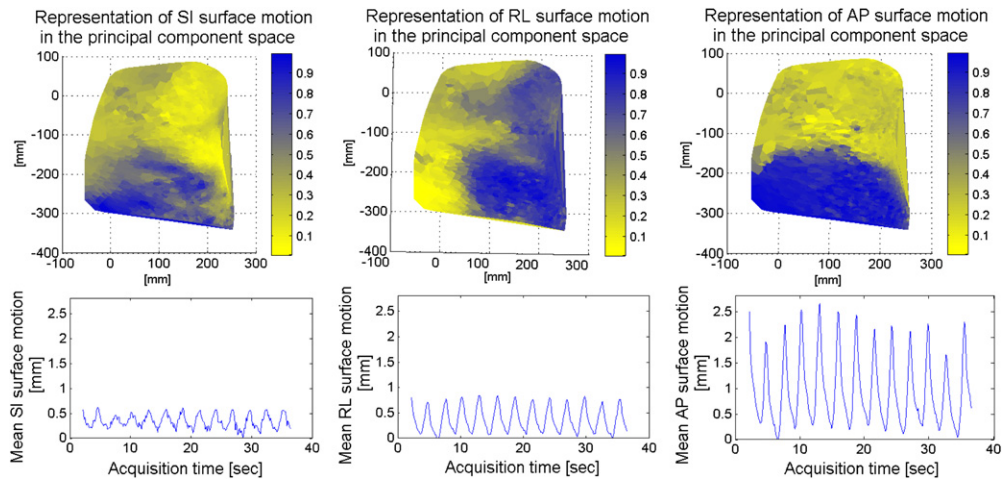


**Figure 10.** The lower panels depict the breathing motion of the patient's thoraco-abdominal surface along SI, RL and AP directions, computed from the 3D average coordinates of the estimated corresponding surface points. The upper panels show the spatial representation of the multi-dimensional surface motion in the principal component space, depicting for each surface point the first principal component score obtained by applying PCA analysis on the point trajectories in the three directions. Surface points with high scores strongly contribute to the breathing motion in that specific direction.

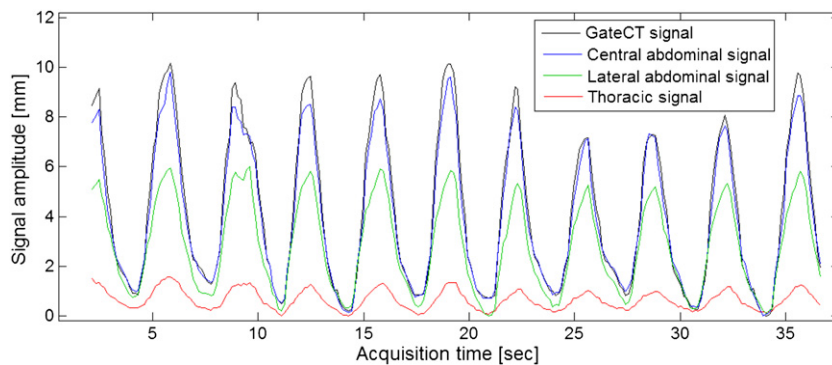


**Figure 11.** Comparison between the acquired GateCT signal and the estimated AP motion of three surface points selected on the thorax and on the central and lateral areas of the abdomen. The central abdominal signal correctly follows the GateCT signal, which was obtained by choosing the surface patch on the central part of the abdomen. The lower correlation between the GateCT and the lateral abdominal signal shows the potential variability of the external surface motion.

the developed registration algorithm were evaluated on five healthy subjects, using a state of the art surface imaging system to acquire the thoraco-abdominal surface at different breathing phases. Due to specific technical limitations of the employed optical system, tracking errors could be assessed only on static surface acquisitions. For meshes dynamically acquired at high frame rates, the AlignRT system does not provide the textured information used to compute the ground truth position of the control points. The designed static validation of the registration algorithm covered however the whole range of surface motion for each test subject, since surfaces were acquired by sampling the breathing cycle at the extreme and intermediate phases.

The implemented algorithm showed a residual distance between the deformed source and the target meshes, expressed as 95% confidence intervals for the measured distance, below 1.20 mm for all subjects. A further analysis of the registration accuracy was performed using star-shaped markers placed on the thoraco-abdominal surface of the subjects. The ground truth position of the landmarks was manually identified on the acquired textured surfaces. The median errors in motion tracking by means of deformable mesh registration proved to be 1.61 mm. The performance of the developed deformable approach was significantly superior to rigid procedures, both in terms of surface overlap and marker localization errors. Rigid surface registration yielded in fact an increase in the distance between corresponding landmarks on the source and target mesh with respect to the initial condition, although the overall surface distance was slightly reduced. These results support the need for non-rigid registration procedures when dealing with thoraco-abdominal surfaces, in order to adequately account for the deformation due to breathing motion.

A critical aspect that may negatively influence the accuracy of surface registration applied to the thoraco-abdominal area is the low spatial frequency of the surfaces due to lack of geometrical features. Mesh registration was therefore performed without selecting any region of interest, since the decrease of spatial constraints due to the smaller patch sizes can lead to surface fitting degeneration, thus reducing registration accuracy. The measured errors in corresponding landmark localization may be partly related also to the intrinsic imprecision of the optical imaging system in 3D surface reconstruction and to the inaccuracies in the identification of the marker position on the textured meshes. An analysis of the intra- and inter-operator variability in the manual selection of the control points was performed. According to the obtained results, we used the position of star centroids as reference variable for method validation, since it featured lower intra- and inter-operator variability with respect to the localization of star vertices. Due to high reproducibility in centroid identification between different operators, the registration errors were computed by considering the ground truth position of the control points defined by a single operator. A sensitivity analysis of the main structural parameters of the registration algorithm was also performed, showing no significant influence on the overall registration accuracy. Slightly worse results were obtained for low numbers of outer iterations and for high final values of the stiffness factor, both contributing to a reduced ability of the surface to deform, i.e. to recover the breathing-induced deformation.

A more detailed analysis of the registration performance as a function of marker positions revealed that localization errors are significantly different for the thoracic and the abdominal regions, featuring a high correlation with the surface motion in the SI direction. As depicted in figure 12, the implemented registration algorithm can correctly estimate the AP motion of the abdominal surface portion but mostly fails to recover the thoracic breathing motion in the SI direction. The registration errors in localizing markers on the abdominal regions were 1.09 mm, with the most relevant component along the RL direction, whereas thoracic control points showed localization errors of 2.13 mm, mainly associated with the SI direction.

The limited ability of the registration algorithm in estimating the SI surface motion can be partly explained by the acquisition procedure with the commercial surface imaging system used for the analysis. Since surface motion along the SI and RL axes is normal to the direction of the projected structured light pattern, it causes the relative slipping of the pattern with respect to the underlying surface. Displacements in SI and RL directions are consequently more difficult to capture, as confirmed by the separate error analysis for each anatomical direction (figure 8). On the other hand, surface motion in the AP direction may result in apparent displacement in the other two directions, as shown in figure 10 for the clinical data analysis. In this case, the PCA analysis incorrectly suggests that the contribution of surface points to the SI breathing motion is mainly focused in the abdominal region, whereas ground

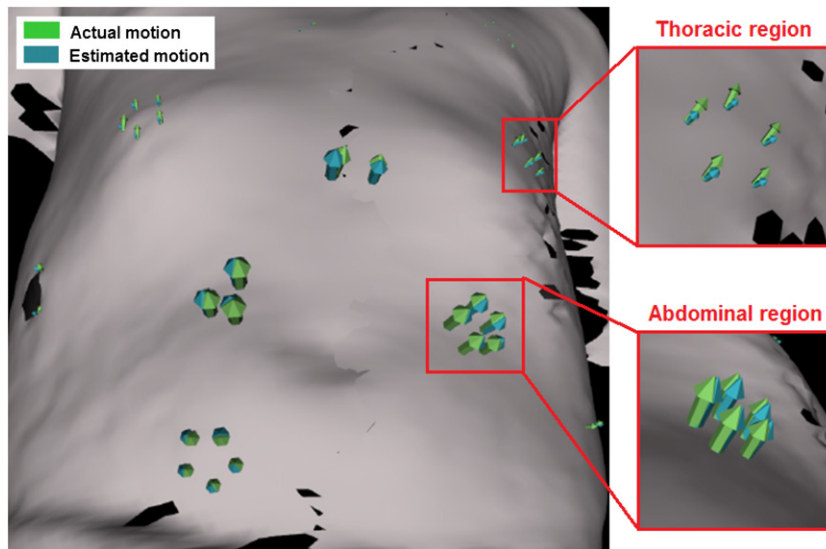


**Figure 12.** Comparison between the actual motion of the thoracic and abdominal surface regions, and the displacement estimated through deformable mesh registration.

truth motion occurs in the AP direction. As a matter of fact, the orientation of the structured light projector with respect to the patient results in sliding of the incident pattern when the surface moves in the AP direction. As can be seen in figure 12, breathing surface motion features larger amplitude in the abdominal region along the AP direction, whereas the thoracic motion component along the SI direction is limited. We can therefore suggest that the reduced accuracy of the implemented registration algorithm in recovering SI surface motion does not represent a critical aspect for clinical applications.

Major concerns are associated with the computational cost of the algorithm, which does not currently provide real-time performance. The mean time required for a single outer iteration is about 9 s, depending on the number of vertices in the registered meshes. The most time-consuming step is the Cholesky factorization of the system matrix, which is performed at each outer iteration, when the point correspondence weights are updated. This limitation derives from the adopted global regularization approach, which involves that each vertex has an influence on every other vertex of the mesh, resulting in a very large linear system that is costly to solve. Future works will be mainly focused on the computational optimization of the method, in order to achieve the real-time performance required for the continuous monitoring of breathing motion during radiotherapy treatments. Multi-resolution strategies and/or a more local regularization approach, using for example a fixed-size vertex neighbourhood or GPU-based techniques, could potentially provide significant speed gains, suitable for real-time applications.

The implemented registration algorithm was also evaluated on real patient data, showing the clinical feasibility in the estimation of a multi-dimensional breathing signal for different thoraco-abdominal regions. The proposed method is put forward to represent a significant improvement for problems dealing with respiratory motion in radiation therapy. The state of the art clinical systems that currently account for breathing movement are limited to a restricted area of the body surface. Such an approach does not accurately depict the complexity of human respiration processes, involving the combined composition of thoracic and abdominal surface

motion. A multi-dimensional respiratory signal accounting for different breathing patterns, as provided by the implemented deformable registration algorithm, could potentially improve current solutions for motion compensated treatment planning and delivery. There is still no evidence that better external motion tracking will lead to a more accurate estimate of the internal tumour position. However, the improved breathing surrogate signal derived from the implemented deformable surface registration is put forward to provide potential benefits for tumour targeting, as long as robust and reliable internal/external correlation models are used. We expect to demonstrate the effective advantages of the proposed approach by using a specifically acquired patient database, which includes the synchronized acquisitions of the external thoraco-abdominal surface and the internal tumour position, derived from cone beam CT projections.

## 5. Conclusion

We showed that deformable mesh registration can be used to recover multi-dimensional breathing motion of the thoraco-abdominal surface from markerless optical surface acquisitions, thus overcoming the lack of surface point correspondence. The accuracy of the implemented registration algorithm in tracking respiratory motion was quantified in five healthy subjects and proved to be site-specific and correlated with the direction of surface displacement. The AP motion in the abdominal region was usually correctly recovered using the registration algorithm, obtaining localization errors of 1.09 mm. Thoracic surface portion showed instead registration errors of 2.13 mm, mainly predominant in the SI direction due to the sliding effect of the projected structured light pattern. Since the most relevant component of the breathing motion is focused in the abdominal region along the AP direction, the limited accuracy of deformable registration in recovering the SI motion of the thorax does not represent a critical aspect for clinical applications. The feasibility of the proposed approach in extracting a multi-dimensional respiratory signal for different anatomical regions was assessed on real patient data, using a clinically available markerless optical system. The implemented deformable registration method is put forward to represent a significant improvement in the management of respiratory motion in radiotherapy, especially for the reduction of motion artefacts in 4D planning images and for the compensation of tumour motion based on internal/external correlation models. A particularly interesting application may be to combine the respiratory signal extracted from the thorax surface motion with a patient-specific breathing model directly built from 4DCT planning images (Vandemeulebroucke *et al* 2011), for the non-invasive estimation of the lesion position. The developed approach may also complement state of the art surface imaging devices with 3D motion tracking of selected surface landmarks.

## Acknowledgments

The authors acknowledge the European project ULICE (Union of Light Ion Centers in Europe, FP7-INFRA-2008-1.1.2) for its support and funding. The authors would also like to thank the volunteers for their participation.

## References

- Allen B, Curless B and Popović Z 2003 The space of human body shapes: reconstruction and parameterization from range scans *ACM Trans. Graph.* **22** 587–94
- Amberg B, Romdhani S and Vetter T 2007 Optimal step nonrigid ICP algorithms for surface registration *Proc. IEEE Conf. Comp. Vis. Patt. Recog. (Minneapolis, MN)* pp 1–8

- Baroni G, Garibaldi C, Riboldi M, Spadea M F, Catalano G, Tagaste B, Tosi G, Orecchia R and Pedotti A 2006 3D optoelectronic analysis of interfractional patient setup variability in frameless extracranial stereotactic radiotherapy *Int. J. Radiat. Oncol. Biol. Phys.* **64** 635–42
- Bert C, Metheany K G, Doppke K and Chen G T 2005 A phantom evaluation of a stereo-vision surface imaging system for radiotherapy patient setup *Med. Phys.* **32** 2753–62
- Besl P and McKay N 1992 A method for registration of 3-D shapes *IEEE Trans. Pattern Anal. Mach. Intell.* **14** 239–56
- Brahme A, Nyman P and Skatt B 2008 4D laser camera for accurate patient positioning, collision avoidance, image fusion and adaptive approaches during diagnostic and therapeutic procedures *Med. Phys.* **35** 1670–81
- Depuydt T *et al* 2011 Geometric accuracy of a novel gimbals based radiation therapy tumor tracking system *Radiother. Oncol.* **98** 365–72
- Feldmar J and Ayache N 1996 Rigid, affine and locally affine registration of free-form surfaces *Int. J. Comput. Vis.* **18** 99–119
- Ford E, Mageras G, Yorke E, Rosenzweig K E, Wagman R and Ling C C 2002 Evaluation of respiratory movement during gated radiotherapy using film and electronic portal imaging *Int. J. Radiat. Oncol. Biol. Phys.* **52** 522–31
- Gianoli C, Riboldi M, Spadea M F, Travaini L L, Ferrari M, Mei R, Orecchia R and Baroni G 2011 A multiple points method for 4D CT image sorting *Med. Phys.* **38** 656–67
- Hoogeman M, Prévost J B, Nuytens J, Pöll J, Levendag P and Heijmen B 2009 Clinical accuracy of the respiratory tumor tracking system of the cyberknife: assessment by analysis of log files *Int. J. Radiat. Oncol. Biol. Phys.* **74** 297–303
- Ibáñez L, Schroeder W, Ng L, Cates J and Insight Software Consortium 2005 *The ITK Software Guide* 2nd edn (updated for ITK version 2.4) (New York: Kitware)
- Keall P J *et al* 2006 The management of respiratory motion in radiation oncology report of AAPM Task Group 76 *Med. Phys.* **33** 3874–900
- Kilby W, Dooley J R, Kuduvali G, Sayeh S and Maurer C R 2010 The CyberKnife Robotic Radiosurgery System in 2010 *Technol. Cancer Res. Treat.* **9** 433–52
- Meeks S L, Tomé W A, Willoughby T R, Kupelian P A, Wagner T H, Buatti J M and Bova F J 2005 Optically guided patient positioning techniques *Semin. Radiat. Oncol.* **15** 192–201
- Moser T, Fleischhacker S, Schubert K, Sroka-Perez G and Karger C P 2011 Technical performance of a commercial laser surface scanning system for patient setup correction in radiotherapy *Phys. Med.* **27** 224–32
- Schroeder W, Martin K and Lorensen B 2006 *The Visualization Toolkit: An Object-Oriented Approach to 3D Graphics* 4th edn (New York: Kitware)
- Vandemeulebroucke J, Rit S, Kybic J, Clarysse P and Sarrut D 2011 Spatiotemporal motion estimation for respiratory-correlated imaging of the lungs *Med. Phys.* **38** 166–78
- Verellen D, Depuydt T, Gevaert T, Linthout N, Tournel K, Duchateau M, Reynders T, Storme G and De Ridder M 2010 Gating and tracking, 4D in thoracic tumours *Cancer Radiother.* **14** 446–54
- Wagner T H, Meeks S L, Bova F J, Friedman W A, Willoughby T R, Kupelian P A and Tome W 2007 Optical tracking technology in stereotactic radiation therapy *Med. Dosim.* **32** 111–20
- Wang L T, Solberg T D, Medin P M and Boone R 2001 Infrared patient positioning for stereotactic radiosurgery of extracranial tumors *Comput. Biol. Med.* **31** 101–11